



**HAL**  
open science

## Basin-scale biogeochemical and ecological impacts of islands in the tropical Pacific Ocean

Monique Messié, Anne Petrenko, Andrea M. Doglioli, Elodie Martinez,  
Séverine Alvain

► **To cite this version:**

Monique Messié, Anne Petrenko, Andrea M. Doglioli, Elodie Martinez, Séverine Alvain. Basin-scale biogeochemical and ecological impacts of islands in the tropical Pacific Ocean. *Nature Geoscience*, 2022, 15, pp.469-474. 10.1038/s41561-022-00957-8 . insu-03779397

**HAL Id: insu-03779397**

**<https://insu.hal.science/insu-03779397>**

Submitted on 22 Dec 2022

**HAL** is a multi-disciplinary open access archive for the deposit and dissemination of scientific research documents, whether they are published or not. The documents may come from teaching and research institutions in France or abroad, or from public or private research centers.

L'archive ouverte pluridisciplinaire **HAL**, est destinée au dépôt et à la diffusion de documents scientifiques de niveau recherche, publiés ou non, émanant des établissements d'enseignement et de recherche français ou étrangers, des laboratoires publics ou privés.

1 *This version of the article has been accepted for publication, after peer review and is subject to*  
2 *Springer Nature's AM terms of use, but is not the Version of Record and does not reflect post-*  
3 *acceptance improvements, or any corrections. The Version of Record is available online at:*  
4 <https://doi.org/10.1038/s41561-022-00957-8> (full text: <https://rdcu.be/cO4qr>)

5 Citation: Messié, M., Petrenko, A., Doglioli, A.M., Martinez, E., and Alvain, S. Basin-scale  
6 biogeochemical and ecological impacts of islands in the tropical Pacific Ocean. *Nat. Geosci.* 15,  
7 469–474 (2022). <https://doi.org/10.1038/s41561-022-00957-8>

8

9

10 Basin-scale biogeochemical and ecological impacts of islands in the  
11 tropical Pacific Ocean

12

13 M. Messié<sup>1,2,\*</sup>, A. Petrenko<sup>2</sup>, A. Doglioli<sup>2</sup>, E. Martinez<sup>3</sup>, and S. Alvain<sup>4</sup>

14

15 <sup>1</sup>Monterey Bay Aquarium Research Institute, Moss Landing, CA 95039, USA

16 <sup>2</sup>Aix Marseille Univ, Université de Toulon, CNRS, IRD, MIO, Marseille, France

17 <sup>3</sup>University of Brest, Ifremer, CNRS, IRD, Laboratoire d'Océanographie Physique et Spatiale  
18 (LOPS), IUEM, 29200 Brest, France

19 <sup>4</sup>Laboratoire d'Océanologie et de Géosciences, UMR 8187 – LOG, CNRS, Université de Lille,  
20 Université du Littoral Côte d'Opale, Wimereux, France

21 \*corresponding author, [monique@mbari.org](mailto:monique@mbari.org)

22

23 **In the relatively unproductive waters of the tropical ocean, islands can enhance**  
24 **phytoplankton biomass and create hotspots of productivity and biodiversity that sustain**  
25 **upper trophic levels, including fish that are crucial to the survival of islands' inhabitants.**  
26 **This phenomenon, coined the "island mass effect" sixty-five years ago, has been widely**  
27 **described. However, most studies focused on individual islands, and very few documented**  
28 **phytoplankton community composition. Consequently, basin-scale impacts on**  
29 **phytoplankton biomass, primary production, and biodiversity remain largely unknown.**  
30 **Here we systematically identify enriched waters near islands from satellite chlorophyll**  
31 **concentration (a proxy for phytoplankton biomass) to analyze the island mass effect for all**  
32 **tropical Pacific islands on a climatological basis. We find enrichments near 99% of islands,**  
33 **impacting 3% of the tropical Pacific Ocean. We quantify local and basin-scale increases in**  
34 **chlorophyll and primary production by contrasting island-enriched waters with nearby**  
35 **waters. We also unveil, for the first time, a significant impact on phytoplankton community**  
36 **structure and biodiversity visible in anomalies in the ocean color signal. Our results suggest**  
37 **that, in addition to strong local biogeochemical impacts, islands may have even stronger**  
38 **and further reaching ecological impacts.**

39 Phytoplankton, the tiny drifting algae that fix carbon dioxide via photosynthesis, are responsible  
40 for about half of the world's primary production<sup>1</sup> and support essentially all life in the open  
41 ocean. Their community composition and biodiversity have been tied to vertical carbon export,  
42 resource use efficiency, and ecological stability<sup>2,3,4</sup>. As such, phytoplankton biomass, production,  
43 and biodiversity have far-reaching impacts on marine ecosystems and the global carbon cycle. It  
44 is thus paramount to understand their environmental drivers so as to predict, and potentially  
45 mitigate, how they may change in the future. In most of the tropical ocean, nutrient supply is the

46 primary factor limiting phytoplankton growth<sup>5</sup>. Far from continents, nutrients are brought to the  
47 sunlit surface layer primarily by vertical mixing<sup>6</sup>, wind- and eddy-driven upwelling<sup>7</sup>, atmospheric  
48 deposition<sup>8</sup>, nitrogen fixation<sup>9</sup>, and horizontal advection<sup>10</sup>. Phytoplankton biodiversity is difficult  
49 to monitor; its patterns and drivers remain largely unknown even when focusing on the simplest  
50 of biodiversity metrics, richness (number of coexisting species). Several studies found high  
51 richness in warm, stable tropical regions and identified temperature as the primary phytoplankton  
52 richness driver<sup>11,12</sup>. Others described increased richness in dynamic regions<sup>13</sup>, highlighting  
53 drivers such as nutrient supply rate and composition, advection, and top-down control<sup>14</sup>.

54 Here, we focus on a phenomenon that has paradoxically received little attention at the basin  
55 scale, despite its prevalence and strong local impacts: island-driven increases in phytoplankton  
56 production, resulting in nearly ubiquitous chlorophyll enrichments near tropical Pacific islands  
57 and atolls<sup>15</sup>. This “island mass effect” (IME)<sup>16</sup> can result from various processes such as  
58 upwelling and mixing in lee eddies, island runoff, submarine groundwater discharge, and others  
59 (reviewed by Gove et al.<sup>15</sup>). These processes supply additional nutrients relative to surrounding  
60 waters, supporting enhanced phytoplankton growth and dramatically increasing local  
61 productivity. The resulting increased fish production is crucial to Pacific island societies that rely  
62 on fishing for food security and protein intake<sup>17</sup>. By increasing primary production, islands can  
63 also locally create an important oceanic sink for atmospheric CO<sub>2</sub> (as observed in the Southern  
64 Ocean<sup>18</sup>) and have been hypothesized to significantly contribute to the global carbon budget<sup>19</sup>.

65 IMEs have been described for a few of the thousands of tropical Pacific islands, notably the  
66 Galapagos<sup>20</sup>, Hawaii<sup>21</sup>, the Marquesas<sup>22</sup>, Kiribati<sup>23</sup>, Solomon<sup>24</sup>, New Caledonia<sup>25</sup>, Tonga<sup>26</sup>,  
67 Vanuatu, and Fiji<sup>27</sup>. There are also some rare reports of island impacts on phytoplankton  
68 community composition<sup>28,29,30</sup>. Only two studies systematically investigated the IME for several

69 islands at once: a compilation of *in situ* chlorophyll concentration in the south tropical Pacific<sup>27</sup>,  
70 and an analysis of satellite chlorophyll increase near 35 coral reef islands and atolls<sup>15</sup>. Neither  
71 study considered phytoplankton community composition. A systematic study of the IME for all  
72 islands in the tropical Pacific, particularly addressing impacts on phytoplankton biodiversity, is  
73 unprecedented.

## 74 **Characterizing island mass effects in the tropical Pacific**

75 We investigated the IME for all tropical Pacific islands and shallow reefs using satellite surface  
76 chlorophyll concentrations (hereafter Chl). A total of 11,449 islands and 4,602 shallow reefs  
77 were identified from high-resolution coastline and bathymetry. Islands and reefs were combined  
78 within land pixels of the 4 km resolution Chl grid (pixels shallower than 30 m were treated as  
79 land, see Methods), resulting in a database of 437 islands and 227 shallow reefs (hereafter  
80 “islands”). An algorithm automatically detecting IMEs from Chl maps was developed and  
81 applied both to the time-averaged Chl and to a monthly climatology. For each island, the  
82 algorithm identified the IME as a Chl contour enclosing the island and surrounding high-Chl  
83 waters, termed IME region. A reference (REF) region of the same size was detected alongside  
84 each IME region, enclosing nearby non-IME waters (Extended Fig. 1). The REF region  
85 represents conditions that would exist if no IME was present. Increases in Chl nearby islands and  
86 within the IME regions were defined relative to REF.

87 The algorithm detected IMEs for most islands, whether in oligotrophic gyres or in more  
88 productive equatorial regions. Islands with the strongest, most far-reaching impacts on average  
89 Chl include the Marquesas, Fiji/Tonga, Solomon, Kiribati, and the Galapagos (Fig. 1). Most  
90 IMEs are strongly seasonal, such that an average map does not adequately render the IME

91 prevalence or strength. When applied to climatological maps (Fig. 1 inserts), the method detected  
92 an IME near 99% of islands (Table 1). Some of these IMEs only represent weak Chl increases  
93 because climatological averages smooth the IME signal, but their presence indicates that an IME  
94 likely occurred during the satellite time period. A more conservative approach still identified  
95 IMEs near 90% of islands (right column). If anything, the IME prevalence may be  
96 underestimated as small IMEs may not be detected using a 4-km resolution product (see Table  
97 S1). This confirms that the IME is nearly ubiquitous in the tropical Pacific<sup>15</sup>. Overall, our results  
98 indicate that the IME impacts 3% of the tropical Pacific area although islands and reefs together  
99 only represent 0.4%.

## 100 **Island impacts on phytoplankton biomass and production**

101 Local IME impacts were assessed by comparing the paired IME and REF regions, and total  
102 impacts calculated by summing the results over the entire tropical Pacific for each climatological  
103 month and averaging over time. The results reveal a strong impact of islands on surface  
104 phytoplankton biomass (using Chl as a proxy) and on satellite-derived primary production<sup>31</sup>  
105 (Table 1). Chl increases by 9% and primary production by 3% on average within IME regions.  
106 Next to the islands, impacts are even more dramatic with a Chl increase of 26% on average. The  
107 apparent higher impact on Chl than primary production is partially due to the lower spatial  
108 resolution of the primary production product (9 km vs 4 km for Chl), combined with the fact that  
109 pixels closest to islands, where impacts are greatest, must be removed (see Methods).

110 While local impacts are very high, islands seem to increase Chl and primary production by less  
111 than 1% over the tropical Pacific (Table 1). These numbers may be underestimated because of  
112 removing shallow pixels near islands where impacts are greatest, and because our algorithm

113 misses delayed IMEs occurring offshore<sup>26</sup> by assuming that the IME region is connected to the  
114 island. Although Chl measured by satellites is only representative of approximately a fifth of the  
115 euphotic zone, the relative impact on total vertically integrated phytoplankton biomass may be  
116 expected to be of the same order of magnitude as the impact on Chl since IME enrichments  
117 typically occur over the full euphotic zone<sup>15</sup>.

118 The overall primary production increase around 0.05 PgC/yr (Table 1) can be compared to other  
119 processes, for which regional estimates of the nitrate supply carbon-equivalent (potential new  
120 production) are available. Potential new production represents an upper bound for new  
121 production, itself representing less than half of primary production in the region<sup>32</sup>, which  
122 provides a basis for rough comparisons with the IME even though island-induced nutrient supply  
123 is unknown. These other processes include wind-driven upwelling (1.8 to 3.9 PgC/yr including  
124 equatorial upwelling when adapting past results to the region<sup>33</sup>), turbulent vertical mixing at the  
125 nitracline (0.4 PgC/yr for the region<sup>6</sup>), nitrogen fixation (around 0.2 PgC/yr for the Pacific<sup>34</sup>,  
126 noting that nitrogen fixation may be partly supported by IMEs<sup>28,26</sup>), and the Peru upwelling  
127 system (0.1 PgC/yr<sup>35</sup>). Consequently, despite strong local impacts, islands are unlikely to  
128 represent a major source of nutrients for phytoplankton in the tropical Pacific and to play an  
129 important role in the global carbon budget.

### 130 **Island impacts on phytoplankton taxonomy**

131 Assessing island impacts on phytoplankton species composition is a challenging proposition.  
132 There is at present no *in situ* dataset with the taxonomic and spatiotemporal coverage needed to  
133 describe phytoplankton community structure and biodiversity throughout the tropical Pacific.  
134 Significant progress has been made towards identifying phytoplankton taxonomy from space<sup>36</sup>,

135 but published methods only identify a small number of broad taxonomic groups or size classes.  
136 To circumvent the lack of taxonomic resolution in satellite products, we used PHYSAT<sup>37</sup>, a  
137 method clustering anomalies in the ocean color signal into 61 phenological bio-optical classes<sup>38</sup>  
138 (hereafter phenoclasses, see Methods). Because phytoplankton characteristics such as cell size,  
139 composition, intracellular structure, cell arrangement, and absorption impact the ocean color  
140 signal, phenoclasses are representative of various phytoplankton communities<sup>39</sup>. We applied  
141 classical ecological metrics to phenoclasses, capturing changes in phenoclass composition and  
142 diversity between IME and REF regions. These ecological metrics describe island-driven  
143 changes in phenoclasses, themselves revealing changes in phytoplankton taxonomy.

144 Island impacts on phytoplankton community composition were studied using the Bray-Curtis  
145 dissimilarity index applied to phenoclasses (Fig. 2a). High phenoclass dissimilarity was  
146 identified between IME and REF regions for most islands, particularly at low latitudes,  
147 suggesting a strong island impact on phytoplankton community composition. These differences  
148 are considerably higher than between random sets of pixels encompassing the IME and REF  
149 regions (Fig. 3a left), confirming that they are significant and not due to random spatial  
150 heterogeneity in PHYSAT phenoclasses. We looked more closely at the most common  
151 phenoclasses found in the tropical Pacific. These are part of “labeled” phenoclasses that were  
152 matched to dominant broad taxonomic groups thanks to coincident in situ data. The  
153 corresponding phytoplankton groups are mostly *Prochlorococcus*, followed by nanoplankton and  
154 *Synechococcus*, consistent with known phytoplankton composition in the region<sup>40</sup>.

155 *Prochlorococcus*-labeled phenoclasses significantly decreased in proportion within the IME  
156 region relative to REF, while *Synechococcus*- and nanoplankton-labeled phenoclasses both

157 increased, albeit non-significantly for nanoplankton (Fig. 3a right). This is coherent with reports  
158 of *Synechococcus* and nanoplankton outcompeting *Prochlorococcus* at higher nutrient levels<sup>41,42</sup>.

159 Island impacts on phytoplankton biodiversity were investigated using several dimensions of  
160 phenoclass diversity: richness (number of distinct phenoclasses), evenness (phenoclass  
161 proportion homogeneity), and the Shannon index, a widely used biodiversity metric that accounts  
162 for both richness and evenness (Table 1). On average, phenoclass richness strongly increases  
163 near islands, more than Chl and primary production. The island-driven phenoclass richness  
164 increase is spatially variable (Fig. 2b), highest poleward of 10° latitude in both hemispheres.

165 There is no impact on evenness, and a smaller impact on Shannon diversity. Part of the richness  
166 increase simply arises because, by definition, Chl is higher in IME than REF regions (Fig. 3b,  
167 left). Indeed, phenoclass richness is strongly correlated with Chl ( $r = 0.72$  across REF regions,  
168 Extended Fig. 3), consistent with *in situ* phytoplankton richness patterns in low productivity  
169 waters<sup>43</sup>. However, the island-driven increase in phenoclass richness is only weakly correlated to  
170 the Chl increase ( $r = 0.22$ ), suggesting that this Chl signal only explains part of the phenoclass  
171 richness increase. We randomly selected two thirds of the IME and REF regions with similar Chl  
172 characteristics, effectively removing the Chl signal (Extended Fig. 4). A total of 1,000 random  
173 permutations were selected, and 33% of permutations still displayed significantly higher  
174 phenoclass richness within the IME subset (Fig. 3b, right). Taken together, these results suggest  
175 that the observed island-driven increase in phenoclass richness is not only linked to increased  
176 Chl, but also partly due to some island-specific phenomenon. We hypothesize that some islands  
177 release nutrients with ratios different from the ones of ambient waters, depending on soil  
178 composition and human activities, which could favor different species and increase  
179 phytoplankton richness<sup>14</sup>. By contrast, weaker taxonomic impacts would be expected near

180 seamounts<sup>44</sup>, because seamount-driven enrichments result from upwelling and mixing<sup>45</sup> of water  
181 masses close to Redfield ratios.

182 Our satellite-based findings provide compelling evidence for a strong IME impact on  
183 phytoplankton community composition and biodiversity. While PHYSAT is only a proxy for  
184 phytoplankton taxonomy, our results match previous reports from the Marquesas islands,  
185 including a shift from *Prochlorococcus* to *Synechococcus* and an increase in phytoplankton  
186 biodiversity leeward of the islands<sup>29,30</sup>. This island-driven increase in phytoplankton biodiversity  
187 may be a crucial piece contributing to islands being biodiversity hotspots in the world oceans<sup>46</sup>.  
188 Island effects could also contribute to the observed latitudinal maximum phytoplankton richness  
189 in the tropics<sup>11,12</sup>, since islands can export biodiversity to surrounding waters<sup>46</sup>. Observations of  
190 phytoplankton taxonomy around other islands are needed to confirm PHYSAT-inferred island  
191 impacts on phytoplankton community composition and biodiversity.

192 Regardless of impacts on phytoplankton taxonomy, local impacts on biomass and productivity  
193 are so high that regions enriched by IMEs represent oases in an otherwise largely unproductive  
194 environment (Fig. 1). There is strong evidence that they attract fish and marine predators<sup>47,48</sup>, and  
195 represent important stopovers along marine migration corridors<sup>49</sup>. While fishery data would be  
196 biased for islands (due to confounding effects of higher fish biomass and proximity), a recent  
197 study of seamounts found a more than doubled fish catch at seamounts with Chl enhancements  
198 relative to seamounts without<sup>45</sup>. Some islands such as Hawaii and the Galapagos also represent  
199 key conservation sites deemed irreplaceable because of the presence of endemic marine  
200 species<sup>50</sup>. This suggests that islands have profound ecological consequences both at the local and  
201 basin scale, even though large-scale impacts on primary production appear to be small.

202

## 203 **Acknowledgements**

204 M.M. was funded by the European Union’s Horizon 2020 research and innovation programme  
205 under the Marie Skłodowska-Curie grant agreement SAPPHERE No. 746530, and by the David  
206 and Lucile Packard Foundation. The project leading to this publication has received funding from  
207 European FEDER Fund under project 1166-39417 (M.M., A.P., A.D.). We thank Anne-Hélène  
208 Rêve-Lamarche and David Dessailly for their help extracting and using the PHYSAT outputs,  
209 and Eric Pape for useful comments and text edits. The box plots in Fig. 3 were generated using  
210 the IoSR Matlab toolbox (<https://github.com/IoSR-Surrey/MatlabToolbox>), and maps displayed  
211 using m\_map (<https://www.eoas.ubc.ca/~rich/map.html>).

## 212 **Author Contributions Statement**

213 M.M. conceived and designed the study, with input from A.P., A.D., and S.A. M.M. developed  
214 the IME algorithm with input from A.P. and A.D., performed the data analyses, and led the  
215 interpretations and writing. S.A. provided the PHYSAT outputs. A.P., A.D., E.M., and S.A.  
216 provided significant input on the text, and contributed to discussions that shaped the study and  
217 the manuscript.

## 218 **Competing Interests Statement**

219 The authors declare no competing interests.

220 **Tables**

	All IMEs	IMEs with Chl increase nearby islands $\geq 10\%$
<b>IME prevalence</b>		
Percentage of islands with IME detected at least one month a year	98.9%	90.1%
... at least 6 months a year	93.2%	55.1%
... year-long	44.3%	23.9%
Percentage of IME detections over all possible cases (664 islands, 12 months)	83.7%	54.2%
<b>IME spatial impact</b>		
Average IME area	8,001 km <sup>2</sup>	13,558 km <sup>2</sup>
Total IME area within the tropical Pacific (in percentage)	3,179,873 km <sup>2</sup> (3.2%)	3,033,672 km <sup>2</sup> (3.1%)
<b>IME impact on surface chlorophyll concentration (Chl)</b>		
Average nearby percentage Chl increase (pixels closest to island)	25.6%	40.8%
Average percentage Chl increase per IME	9.3%	13.1%
Average total Chl increase per IME (summed over the IME area)	0.21 tons/m	0.37 tons/m
Total IME-induced Chl increase in the tropical Pacific (in percentage)	83 tons/m (0.68%)	82 tons/m (0.67%)
<b>IME impact on primary production (PP)</b>		
Average percentage PP increase per IME	2.8%	4.2%
Average total PP increase per IME (summed over the IME area)	0.14 TgC/yr	0.23 TgC/yr
Total IME-induced PP increase in the tropical Pacific (in percentage)	50.4 TgC/yr (0.51%)	50.2 TgC/yr (0.51%)
<b>IME impact on PHYSAT phenoclass diversity</b>		
Average percentage richness increase per IME	12.1%	13.2%
Average percentage evenness increase per IME	-0.1%	0.0%
Average percentage Shannon index increase per IME	4.1%	4.5%

221 **Table 1: IME impacts in the tropical Pacific.** IME prevalence is defined based on islands  
 222 belonging to an IME region (there can be several islands associated with one IME region).  
 223 “Average” impact refers to impact for a single IME, averaged over all detected IMEs. They  
 224 include both change in ambient conditions in IME vs REF regions, and total island-driven  
 225 increase summed over the IME area. “Total” impact refers to impacts summed over the entire  
 226 study region and averaged over a climatological year. Phenoclass diversity impacts were  
 227 computed for IME/REF regions of at least 100 PHYSAT data points, and richness was

228 normalized to 100 data points to correct for the strong dependence of richness on area sampled  
229 (see Methods). Statistics are given for all IMEs, and for a more conservative subset excluding  
230 those where the island nearby Chl increase was below 10%. Additional metrics (median and  
231 interquartile range) are provided in Extended Table 1.

## 232 **Figure legends**

233 **Figure 1: Map of IME detection in the tropical Pacific.** The main map represents the 2002-  
234 2018 average satellite chlorophyll concentration (MODIS data) in the study region (30°S -  
235 30°N). IME regions are contoured in different shades of red depending on Chl increase nearby  
236 islands relative to a reference region (maximum value in mean conditions: 558% observed for the  
237 Galapagos Islands). Inserts display the climatological month with the highest IME chlorophyll  
238 enrichment in selected regions with a custom color bar: A- Kiribati in May, B- Hawaii in  
239 September, C- Galapagos in January, D- Solomon in July, E- New Caledonia, Vanuatu, Fiji, and  
240 Tonga in February, and F- Marquesas in May. Extended Fig. 2 provides full maps of  
241 climatological months.

242 **Figure 2: Maps of island impacts on PHYSAT phenoclasses, indicative of impacts on**  
243 **phytoplankton community composition and biodiversity.** For each island, the maximum value  
244 observed over the seasonal cycle is displayed (only computed for IME regions containing at least  
245 100 PHYSAT data points). a) Phenoclass Bray-Curtis dissimilarity between IME and REF  
246 regions, indicative of differences in phenoclass composition. b) Phenoclass richness increases in  
247 the IME region relative to REF (richness was normalized to 100 data points). c) Summary of  
248 island impacts on phenoclasses, defined according to the median value for phenoclass Bray-  
249 Curtis dissimilarity (composition, pink) and for richness increase (richness, blue), where  
250 “impacts” are defined as above the median. Phenoclass richness increase is correlated with  
251 absolute latitude ( $r = 0.18$ ) while phenoclass Bray-Curtis dissimilarity is anticorrelated ( $r = -$   
252  $0.24$ ). Despite their opposite relation to latitude, phenoclass richness increase and Bray-Curtis  
253 dissimilarity are actually weakly correlated ( $r = 0.30$ ).

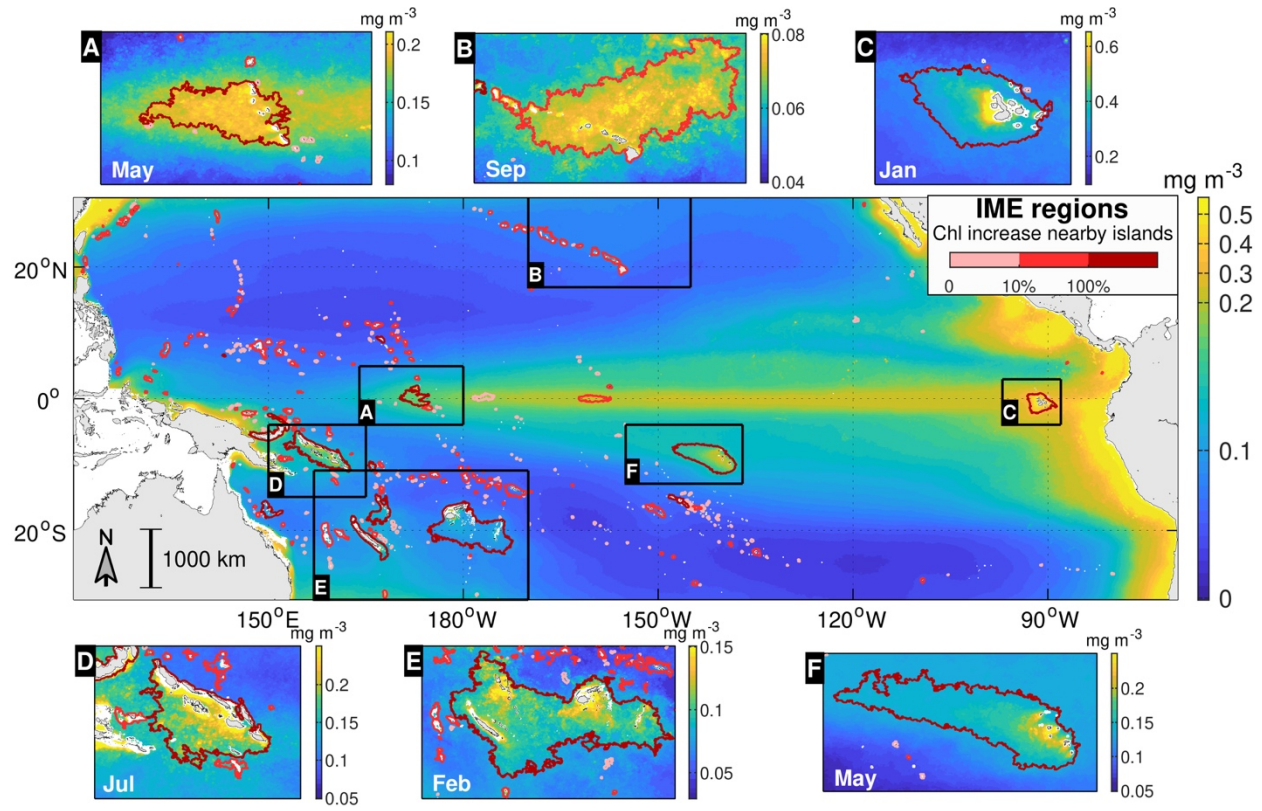
254 **Figure 3: Island impacts on phytoplankton community structure as depicted by PHYSAT.**

255 Statistics are based on paired climatological IME/REF regions with 100 PHYSAT data points  
256 minimum. Box plots report the median (center line), 95% confidence interval around the median  
257 (notches equal to  $\pm 1.58$  times interquartile range divided by square root of the sample size),  
258 interquartile range (box), and 1.5 times the interquartile range (whiskers). Data points are  
259 displayed as crosses (outliers beyond whiskers as dots). Symbols show whether distributions are  
260 statistically different according to a Mann-Whitney U-test (= is non-significant, +/- indicate how  
261 IME medians relate to REF).

262 **a)** Left: Phenoclass Bray-Curtis dissimilarity between IME and REF regions, compared to data  
263 points randomly taken across IME/REF regions. Right: Occurrence frequency of dominant  
264 phenoclasses (frequency  $>0.02$ ) in the IME and REF regions, sorted by label: *Prochlorococcus*  
265 (Pros), *Synechococcus* (Syn), and nanoplankton (Nano).

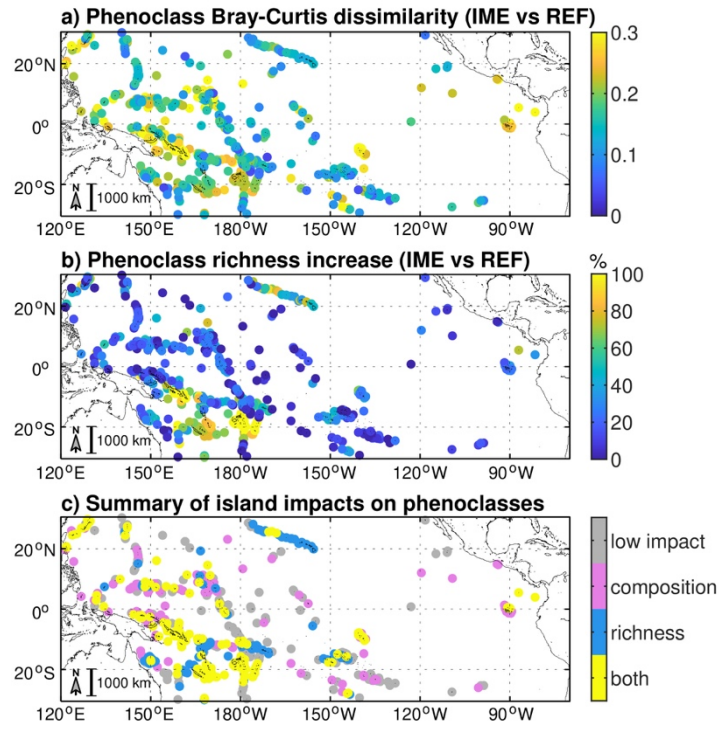
266 **b)** Left 2 panels: Phenoclass richness is significantly higher in IME than in REF regions (9.6%  
267 difference in median) partly linked to higher Chl (12.4% difference in median). Right: summary  
268 of Chl and phenoclass richness characteristics for 1000 random permutations independently  
269 taken within IME and REF regions (N=712) such that their Chl distribution is equivalent  
270 ( $p>0.05$ ). Chl may be insignificantly higher within IME or REF subsets (as described by the  
271 difference in median) because IME/REF pairs are decoupled (example in Extended Fig. 4).

272



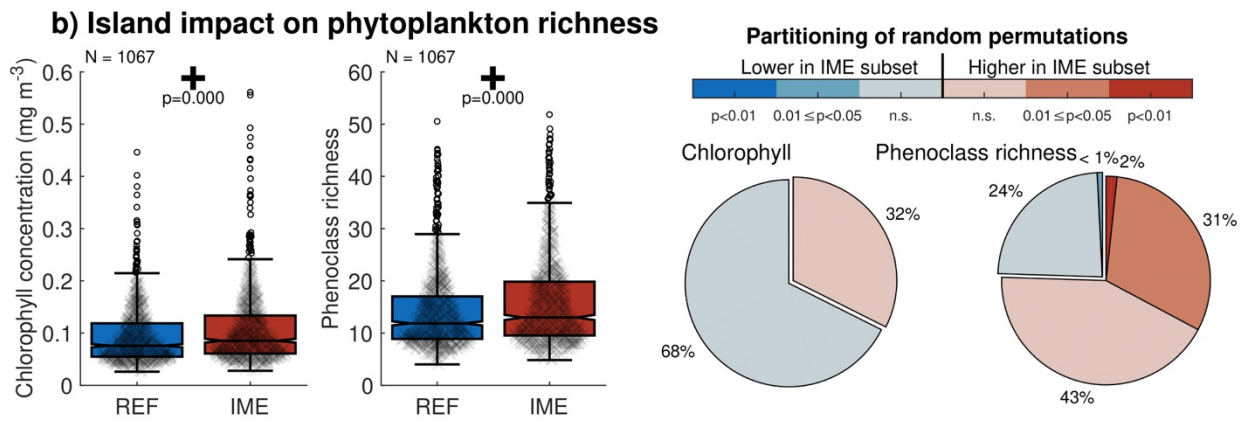
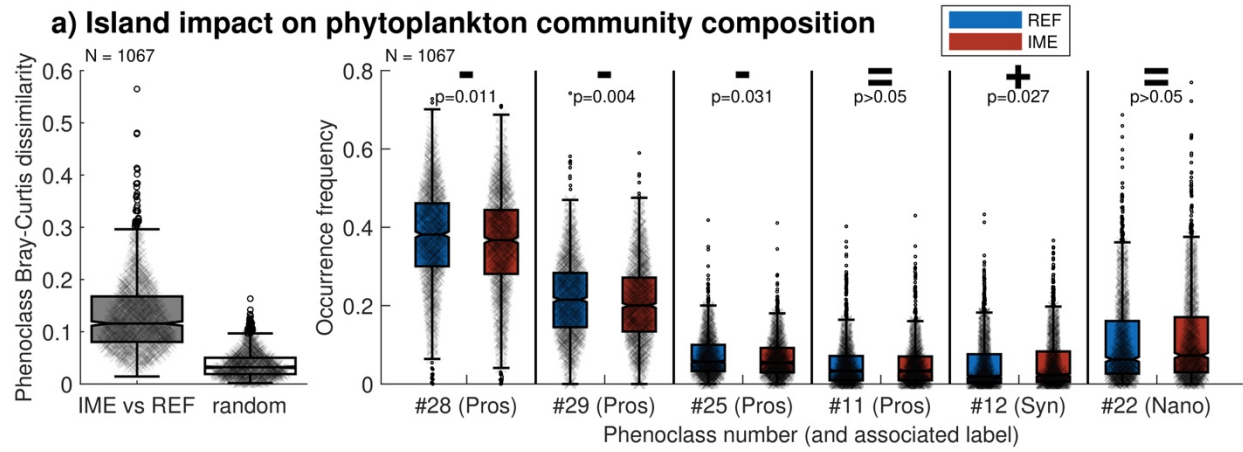
273  
 274  
 275

**Figure 1.**



276  
 277  
 278

**Figure 2.**



279

280

**Figure 3.**

281 **References**

- 282 1. Field, C. B., M. J. Behrenfeld, J. T. Randerson & P. Falkowski (1998), Primary production of  
283 the biosphere: integrating terrestrial and oceanic components, *Science*, 281(5374), 237-240,  
284 <https://doi.org/10.1126/science.281.5374.237>
- 285 2. Guidi, L., S. Chaffron, L., Bittner, D. Eveillard, A. Larhlimi, S. Roux et al. (2016), Plankton  
286 networks driving carbon export in the oligotrophic ocean, *Nature*, 532(7600), 465-470,  
287 <https://doi.org/10.1038/nature16942>
- 288 3. Ptacnik, R., A. G. Solimini, T. Andersen, T. Tamminen, P. Brettum, L. Lepistö, E. Willén &  
289 S. Rekolainen (2008), Diversity predicts stability and resource use efficiency in natural  
290 phytoplankton communities, *Proc. Natl. Acad. Sci.*, 105(13), 5134-5138,  
291 <https://doi.org/10.1073/pnas.0708328105>
- 292 4. Corcoran, A. A. & W. J. Boeing (2012), Biodiversity increases the productivity and stability  
293 of phytoplankton communities, *PLoS ONE*, 7(11), e49397,  
294 <https://doi.org/10.1371/journal.pone.0049397>
- 295 5. Arteaga, L., M. Pahlow & A. Oschlies (2014), Global patterns of phytoplankton nutrient and  
296 light colimitation inferred from an optimality-based model, *Global Biogeochem. Cycles*,  
297 28(7), 648-661, <https://doi.org/10.1002/2013GB004668>
- 298 6. Lewis, M., D. Hebert, W. G. Harrison, T. Platt & N. S. Oakey (1986), Vertical nitrate fluxes in  
299 the oligotrophic ocean, *Science*, 234(4778), 870-873,  
300 <https://doi.org/10.1126/science.234.4778.870>

- 301 7. McGillicuddy, D. J. J., A. A. Laurence, N. R. Bates, T. Bibby, K. O. Buesseler, C. A. Carlson  
302 et al. (2007), Eddy/wind interactions stimulate extraordinary mid-ocean plankton blooms,  
303 Science, 316(5827), 1021-1026, <https://doi.org/10.1126/science.1136256>
- 304 8. Duce, R. A., J. LaRoche, K. Altieri, K. R. Arrigo, A. R. Baker, D. G. Capone et al. (2008),  
305 Impacts of atmospheric anthropogenic nitrogen on the open ocean, Science, 320(5878), 893-  
306 897, <https://doi.org/10.1126/science.1150369>
- 307 9. Tang, W., S. Wang, D. Fonseca-Batista, F. Dehairs, S. Gifford, A. G. Gonzalez et al. (2019),  
308 Revisiting the distribution of oceanic N<sub>2</sub> fixation and estimating diazotrophic contribution to  
309 marine production, Nat. Commun., 10(1), <https://doi.org/10.1038/s41467-019-08640-0>
- 310 10. Letscher, R. T., F. Primeau & J. K. Moore (2016), Nutrient budgets in the subtropical ocean  
311 gyres dominated by lateral transport, Nat. Geosci., 9(11), 815-819,  
312 <https://doi.org/10.1038/ngeo2812>
- 313 11. Righetti, D., M. Vogt, N. Gruber, A. Psomas & N. E. Zimmermann (2019), Global pattern of  
314 phytoplankton diversity driven by temperature and environmental variability, Sci. Adv., 5(5),  
315 eaau6253, <https://doi.org/10.1126/sciadv.aau6253>
- 316 12. Ibarbalz, F. M., Henry, N., Brandão, M. C., Martini, S., Busseni, G., Byrne, H. et al. (2019),  
317 Global trends in marine plankton diversity across kingdoms of life, Cell, 179(5), 1084-  
318 1097.e21, <https://doi.org/10.1016/j.cell.2019.10.008>
- 319 13. Lévy, M., P. J. S. Franks & K. S. Smith (2018), The role of submesoscale currents in  
320 structuring marine ecosystems, Nat. Commun., 9(1), [https://doi.org/10.1038/s41467-018-](https://doi.org/10.1038/s41467-018-07059-3)  
321 [07059-3](https://doi.org/10.1038/s41467-018-07059-3)

- 322 14. Dutkiewicz, S., P. Cermeno, O. Jahn, M. J. Follows, A. E. Hickman, D. A. A. Taniguchi &  
323 B. A. Ward (2020), Dimensions of marine phytoplankton diversity, *Biogeosciences*, 17(3),  
324 609-634, <https://doi.org/10.5194/bg-17-609-2020>
- 325 15. Gove, J. M., M. A. McManus, A. B. Neuheimer, J. J. Polovina, J. C. Drazen, C. R. Smith et  
326 al. (2016), Near-island biological hotspots in barren ocean basins, *Nat. Commun.*, 7, 10581,  
327 <https://doi.org/10.1038/ncomms10581>
- 328 16. Doty, M. S. & M. Oguri (1956), The island mass effect, *J. Cons. Int. Explor. Mer.*, 22(1), 33-  
329 37, <https://doi.org/10.1093/icesjms/22.1.33>
- 330 17. Bell, J. D., M. Kronen, A. Vunisea, W. J. Nash, G. Keeble, A. Demmke, S. Pontifex & S.  
331 Andréfouët (2009), Planning the use of fish for food security in the Pacific, *Marine Policy*,  
332 33(1), 64-76, <https://doi.org/10.1016/j.marpol.2008.04.002>
- 333 18. Bakker, D. C., M. C. Nielsdóttir, P. J. Morris, H. J. Venables & A. J. Watson (2007), The  
334 island mass effect and biological carbon uptake for the subantarctic Crozet Archipelago,  
335 *Deep Sea Research Part II: Topical Studies in Oceanography*, 54(18-20), 2174-2190,  
336 <https://doi.org/10.1016/j.dsr2.2007.06.009>
- 337 19. Heywood, K. J., D. P. Stevens & G. R. Bigg (1996), Eddy formation behind the tropical  
338 island of Aldabra, *Deep Sea Res. Part I*, 43(4), 555-578, [https://doi.org/10.1016/0967-](https://doi.org/10.1016/0967-0637(96)00097-0)  
339 [0637\(96\)00097-0](https://doi.org/10.1016/0967-0637(96)00097-0)
- 340 20. Palacios, D. M. (2002), Factors influencing the island-mass effect of the Galapagos  
341 archipelago, *Geophys. Res. Lett.*, 29(23), 2134, <https://doi.org/10.1029/2002GL016232>

- 342 21. Gilmartin, M. & N. Revelante (1974), The 'island mass' effect on the phytoplankton and  
343 primary production of the Hawaiian Islands, *J. Exp. Mar. Biol. Ecol.*, 16(2), 181-204,  
344 [https://doi.org/10.1016/0022-0981\(74\)90019-7](https://doi.org/10.1016/0022-0981(74)90019-7)
- 345 22. Signorini, S. C., C. R. McClain & Y. Dandonneau (1999), Mixing and phytoplankton bloom  
346 in the wake of the Marquesas Islands, *Geophys. Res. Lett.*, 26(20), 3121-3124,  
347 <https://doi.org/10.1029/1999GL010470>
- 348 23. Messié, M., M.-H. Radenac, J. Lefèvre & P. Marchesiello (2006), Chlorophyll bloom in the  
349 western Pacific at the end of the 1997-98 El Niño: the role of the Kiribati Islands, *Geophys.*  
350 *Res. Lett.*, 33, L14601, <https://doi.org/10.1029/2006GL026033>
- 351 24. Messié, M. & M.-H. Radenac (2006), Seasonal variability of the surface chlorophyll in the  
352 western tropical Pacific from SeaWiFS data, *Deep Sea Res. Part I*, 53(10), 1581-1600,  
353 <https://doi.org/10.1016/j.dsr.2006.06.007>
- 354 25. Le Borgne, R., Y. Dandonneau & L. Lemasson (1985), The problem of the island mass effect  
355 on chlorophyll and zooplankton standing crops around Mare (Loyalty Islands) and New  
356 Caledonia, *Bull. Mar. Sci.*, 37(2), 450-459
- 357 26. Messié, M., A. Petrenko, A. M. Doglioli, C. Aldebert, E. Martinez, G. Koenig, S. Bonnet &  
358 T. Moutin (2020), The delayed island mass effect: How islands can remotely trigger blooms  
359 in the oligotrophic ocean, *Geophys. Res. Lett.*, 47(2), <https://doi.org/10.1029/2019gl085282>
- 360 27. Dandonneau, Y. & L. Charpy (1985), An empirical approach to the island mass effect in the  
361 south tropical Pacific based on sea surface chlorophyll concentrations, *Deep Sea Research*  
362 *Part A*, 32, 707-721, [https://doi.org/10.1016/0198-0149\(85\)90074-3](https://doi.org/10.1016/0198-0149(85)90074-3)

- 363 28. Shiozaki, T., T. Kodama & K. Furuya (2014), Large-scale impact of the island mass effect  
364 through nitrogen fixation in the western South Pacific Ocean, *Geophys. Res. Lett.*, 41(8),  
365 2907-2913, <https://doi.org/10.1002/2014GL059835>
- 366 29. Caputi, L., Q., Carradec, D., Eveillard, A., Kirilovsky, E., Pelletier, J. J. P. Karlusich et al.  
367 (2019), Community-level responses to iron availability in open ocean plankton ecosystems,  
368 *Global Biogeochem. Cycles*, 33(3), 391-419, <https://doi.org/10.1029/2018gb006022>
- 369 30. Martinez, E., M. Rodier, M. Pagano & R. Sauzède (2020), Plankton spatial variability within  
370 the Marquesas archipelago, South Pacific, *J. Mar. Syst.*, 212, 103432,  
371 <https://doi.org/10.1016/j.jmarsys.2020.103432>
- 372 31. Behrenfeld, M. J. & P. G. Falkowski (1997), Photosynthetic rates derived from satellite-  
373 based chlorophyll concentration, *Limnol. Oceanogr.*, 42(1), 1-20,  
374 <https://doi.org/10.4319/lo.1997.42.1.0001>
- 375 32. Laws, E. A., H. Ducklow & J. J. McCarthy (2000), Temperature effects on export production  
376 in the open ocean, *Global Biogeochem. Cycles*, 14(4), 1231-1246,  
377 <https://doi.org/10.1029/1999GB001229>
- 378 33. Messié, M. & F. P. Chavez (2012), A global analysis of ENSO synchrony: the oceans'  
379 biological response to physical forcing, *J. Geophys. Res.*, 117, C09001,  
380 <https://doi.org/10.1029/2012JC007938>
- 381 34. Luo, Y.-W., I. D. Lima, D. M. Karl, C. A. Deutsch & S. C. Doney (2014), Data-based  
382 assessment of environmental controls on global marine nitrogen fixation, *Biogeosciences*,  
383 11(3), 691-708, <https://doi.org/10.5194/bg-11-691-2014>

- 384 35. Messié, M. & F. P. Chavez (2015), Seasonal regulation of primary production in eastern  
385 boundary upwelling systems, *Prog. Oceanogr.*, 134, 1-18,  
386 <https://doi.org/10.1016/j.pocean.2014.10.011>
- 387 36. Mouw, C. B., N. J. Hardman-Mountford, S. Alvain, A. Bracher, R. J. W. Brewin, A. Bricaud  
388 et al. (2017), A Consumer's guide to satellite remote sensing of multiple phytoplankton  
389 groups in the global ocean, *Front. Mar. Sci.*, 4, 41, <https://doi.org/10.3389/fmars.2017.00041>
- 390 37. Alvain, S., C. Moulin, Y. Dandonneau & F. M. Bréon (2005), Remote sensing of  
391 phytoplankton groups in case 1 waters from global SeaWiFS imagery, *Deep Sea Res. Part I*,  
392 52(11), 1989-2004, <https://doi.org/10.1016/j.dsr.2005.06.015>
- 393 38. Rêve-Lamarche, A.-H., S. Alvain, M.-F. Racault, D. Dessailly, N. Guiselin, C. Jamet, V.  
394 Vantrepotte & G. Beaugrand (2017), Ocean Color Radiance Anomalies in the North Sea,  
395 *Front. Mar. Sci.*, <https://doi.org/10.3389/fmars.2017.00408>
- 396 39. Alvain, S., H. Loisel & D. Dessailly (2012), Theoretical analysis of ocean color radiances  
397 anomalies and implications for phytoplankton groups detection in case 1 waters, *Opt.*  
398 *Express*, 20(2), 1070, <https://doi.org/10.1364/oe.20.001070>
- 399 40. Mackey, D. J., J. Blanchot, H. W. Higgins & J. Neveux (2002), Phytoplankton abundances  
400 and community structure in the equatorial Pacific, *Deep Sea Res. Part II*, 49(13-14), 2561-  
401 2582, [https://doi.org/10.1016/S0967-0645\(02\)00048-6](https://doi.org/10.1016/S0967-0645(02)00048-6)
- 402 41. Johnson, Z. I. (2006), Niche partitioning among *Prochlorococcus* ecotypes along ocean-scale  
403 environmental gradients, *Science*, 311(5768), 1737-1740,  
404 <https://doi.org/10.1126/science.1118052>

- 405 42. Martiny, A. C., S. Kathuria & P. M. Berube (2009), Widespread metabolic potential for  
406 nitrite and nitrate assimilation among *Prochlorococcus* ecotypes, *Proc. Natl. Acad. Sci.*,  
407 106(26), 10787-10792, <https://doi.org/10.1073/pnas.0902532106>
- 408 43. Vallina, S. M., M. J. Follows, S. Dutkiewicz, J. M. Montoya, P. Cermeno & M. Loreau  
409 (2014), Global relationship between phytoplankton diversity and productivity in the ocean,  
410 *Nat. Commun.*, 5(1), <https://doi.org/10.1038/ncomms5299>
- 411 44. Dai, S., Y. Zhao, X. Li, Z. Wang, M. Zhu, J. Liang, et al. (2020), The seamount effect on  
412 phytoplankton in the tropical western Pacific, *Mar. Environ. Res.*, 105094,  
413 <https://doi.org/10.1016/j.marenvres.2020.105094>
- 414 45. Leitner, A. B., A. B. Neuheimer & J. C. Drazen (2020), Evidence for long-term seamount-  
415 induced chlorophyll enhancements, *Sci. Rep.*, 10(1), [https://doi.org/10.1038/s41598-020-](https://doi.org/10.1038/s41598-020-69564-0)  
416 [69564-0](https://doi.org/10.1038/s41598-020-69564-0)
- 417 46. Bowen, B. W., L. A. Rocha, R. J. Toonen & S. A. Karl (2013), The origins of tropical marine  
418 biodiversity, *Trends in Ecology & Evolution*, 28(6), 359-366,  
419 <https://doi.org/10.1016/j.tree.2013.01.018>
- 420 47. Worm, B., H. K. Lotze & R. A. Myers (2003), Predator diversity hotspots in the blue ocean,  
421 *Proc. Natl. Acad. Sci.*, 100(17), 9884-9888, <https://doi.org/10.1073/pnas.1333941100>
- 422 48. Block, B. A., I. D., Jonsen, S. J., Jorgensen, S. A., Winship, S. A., Shaffer, S. J. Bograd et al.  
423 (2011), Tracking apex marine predator movements in a dynamic ocean, *Nature*, 475, 86-90,  
424 <https://doi.org/10.1038/nature10082>

- 425 49. Harrison, A.-L., D. P. Costa, A. J. Winship, S. R. Benson, S. J. Bograd, M. Antolos et al.  
426 (2018), The political biogeography of migratory marine predators, *Nature Ecology &*  
427 *Evolution*, 2(10), 1571-1578, <https://doi.org/10.1038/s41559-018-0646-8>
- 428 50. Pompa, S., P. R. Ehrlich & G. Ceballos (2011), Global distribution and conservation of  
429 marine mammals, *Proc. Natl. Acad. Sci.*, 108(33), 13600-13605,  
430 <https://doi.org/10.1073/pnas.1101525108>  
431

## 432 **Methods**

433 **IME detection data sets.** The IME was detected from a climatology of MODIS satellite surface  
434 chlorophyll-*a* concentrations (Chl, 4 km, monthly from July 2002 to December 2018,  
435 erdMHIchlamday product downloaded from  
436 <https://coastwatch.pfeg.noaa.gov/erddap/info/index.html>). The study was based on the 4 km  
437 MODIS Chl grid in the tropical Pacific (30°N/30°S; east/west borders are roughly delimited by  
438 the Americas, Australia, Indonesia, Philippines, and Taiwan, see Fig. 1). Islands were detected  
439 from the Global Self-consistent, Hierarchical, High-resolution Geography Database (GSHHG)  
440 version 2.3.7 full resolution coastline (<https://www.ngdc.noaa.gov/mgg/shorelines/gshhs.html>)  
441 loaded using functions from the m\_map toolbox (<https://www.eoas.ubc.ca/~rich/map.html>).  
442 Bathymetry was obtained from the GEBCO global bathymetry  
443 ([https://www.gebco.net/data\\_and\\_products/gridded\\_bathymetry\\_data/](https://www.gebco.net/data_and_products/gridded_bathymetry_data/)) at 1/15' resolution (< 500  
444 m). A 4 km resolution “shallow mask” was generated for the MODIS grid, including all pixels  
445 containing land shallower than 30 m according to GEBCO or where an island was detected. The  
446 shallow mask was extended by one additional pixel in all directions to ensure that all pixels  
447 containing shallow waters were flagged<sup>15</sup>. All ocean color data (Chl, primary production, and  
448 PHYSAT, see below) were removed within the shallow mask as they were potentially  
449 contaminated by bottom reflectance<sup>15</sup>. In practice, pixels within the shallow mask (containing  
450 land, waters shallower than 30 m, and adjacent pixels) were treated as land.

451 **Island database.** The island database includes both emerged islands and reefs shallower than 30  
452 m according to the GEBCO bathymetry. The reason is that some atolls can have no consistent  
453 (e.g., tide-dependent) or very little emerged land, and can potentially be missed both by GSHHG  
454 and by the GEBCO bathymetry. Islands and reefs were identified as follows. Islands were

455 detected from the GSHHS coastline as closed contours in the 120°E-70°W, 30°S-30°N region.  
456 Because GSHHG was constructed from databases that were built in the 70s and 80s, errors  
457 remained in the location of some islands. Islands being too numerous to all be validated, only  
458 islands from the final database (see below) were checked against GEBCO bathymetry, and where  
459 obvious discrepancies existed, their position was shifted accordingly. The island database was  
460 then reprocessed until no more discrepancy was found (total corrected islands: n=32). The island  
461 database was merged with a published database of 1,779 islands<sup>51</sup> by finding, for each island  
462 from the Nunn et al. database<sup>51</sup>, the closest GSHHS contour. The Nunn et al. database<sup>51</sup> provides  
463 more precise information regarding position, elevation, island type, and area. Last, reefs were  
464 detected from GEBCO (at < 500 m resolution) as groups of pixels shallower than 30 m (“shallow  
465 zones”, n=5,972), that include both submerged reefs and emerged islands. Island and reef  
466 databases were merged by finding islands within shallow zones, when they existed. The  
467 combined dataset after removing contours within the east/west mask (e.g., Atlantic, Indonesia)  
468 includes 16,051 islands and reefs (hereafter “islands”). Islands within 100 km of the tropical  
469 Pacific east/west borders were removed to avoid continental influences (n=5,062). The remaining  
470 islands were then combined within the MODIS shallow mask (see section above and Fig. S1).  
471 The term “island” in the paper thus refers to a group of islands/reefs belonging to a set of  
472 connected shallow pixels. The final database includes 664 islands (437 with emerged lands,  
473 including 363 from the Nunn et al. island database<sup>51</sup>, and 227 shallow reefs).

474 **IME detection.** The IME was defined for each island as the smallest possible Chl contour  
475 enclosing the island that fulfills a list of criteria detailed below (see Fig. S2 for a representation  
476 of the algorithm). Beforehand, the maximum (Chl\_max) and minimum (Chl\_min) nearby Chl  
477 were obtained for each island within a 1-pixel band around the island mask. Islands were ranked

478 by Chl\_min, and processed from lowest to highest Chl\_min. For a given island, the IME Chl  
479 contour (termed cChl) was iteratively lowered by 0.01 mg m<sup>-3</sup> starting at Chl\_max and the  
480 corresponding IME mask computed. The IME mask includes both pixels above cChl and  
481 adjacent missing data, such that other islands can become part of the same IME, then termed  
482 “shared IME”. When this happened, Chl\_max was adjusted to the highest value; Chl\_min does  
483 not need adjustment since islands are processed in Chl\_min order. The iteration was stopped  
484 when one of the following conditions was met: (1) cChl < Chl\_min (the rationale being that  
485 currents displace the nutrient enrichment downstream of the island, so that at least one pixel  
486 surrounding the island should not belong to the IME); (2) the IME mask was too large, either  
487 touching the domain borders, or touching the continent masks or adjacent NaN pixels (this  
488 happens when contours enclose the full oligotrophic gyre); (3) regions of high Chl (>  
489 0.8\*Chl\_max) were found within the IME mask, further than 32 pixels away from any island  
490 (~ 150 km). In this last case, the goal was to avoid non-island sources of nutrients within the IME  
491 region such as open-ocean eddies or upwelling; the 32-pixel tolerance deals with cases where the  
492 Chl maximum is displaced downstream of the islands<sup>52</sup>. The IME peak can occur even further  
493 downstream, notably in cases of delayed IME<sup>26</sup>; 32 pixels thus represents a compromise between  
494 capturing most IMEs and avoiding non-IME local Chl enrichments. While sensitive to the  
495 parameters used, this criterium only concerned 1.3% of cases (for the monthly climatology); in  
496 95% of cases, the algorithm stops due to criterion #2. When one of the 3 criteria was met, a  
497 second iteration was performed at higher resolution (0.001 mg m<sup>-3</sup>) starting with the last cChl  
498 until meeting the criteria again, such that cChl was determined with a 0.001 mg m<sup>-3</sup> accuracy.  
499 This is well beyond measured Chl accuracy, but small changes in cChl can result in large  
500 changes in IME areas on climatological averages, hence the need for high sensitivity. The IME

501 was only kept if the IME mask contained at least 2 Chl pixels. The IME detection algorithm is  
502 available at [https://bitbucket.org/messiem/toolbox\\_IME\\_detection](https://bitbucket.org/messiem/toolbox_IME_detection).

503 **Satellite-derived information on phytoplankton biomass and primary production.** Island  
504 impacts were assessed using satellite chlorophyll-*a* (Chl), a common proxy for phytoplankton  
505 biomass<sup>53</sup> representative of the top ~ 10-30 m in our region (first optical depth). Subsurface  
506 impacts remain unknown; in some cases, apparent surface enrichments can result from the  
507 passive uplift of the deep chlorophyll maximum without any net biomass increase<sup>54</sup>. However, in  
508 situ profiles available near islands suggest this is the exception rather than the rule<sup>15</sup> (see also  
509 Table S3). Island impacts on primary production were estimated using the MODIS-based  
510 standard Vertically Generalized Production Model<sup>31</sup> (VGPM). The VGPM estimates primary  
511 production integrated over the euphotic depth range based on satellite chlorophyll, light  
512 availability, and temperature (a proxy for nutrient availability), and has been widely used for  
513 large-scale studies for which the spatiotemporal coverage of in situ data remains insufficient.  
514 Results are similar when using a more recent primary production algorithm (CAFE model<sup>55</sup>):  
515 total IME-induced PP increase = 44.9 TgC/yr vs 50.4 TgC/yr for the VGPM (Table 1). Primary  
516 production was downloaded from the Ocean Productivity website  
517 (<http://science.oregonstate.edu/ocean.productivity/index.php>) at 9 km resolution for the period  
518 July 2002 - December 2018 (see above for Chl data information). Primary production maps were  
519 averaged into a monthly climatology, pixels shallower than 30 m removed, and data interpolated  
520 on the Chl grid (4 km resolution). The lower resolution of the primary production product means  
521 that areas larger than for Chl were impacted by the shallow pixel removal, effectively removing  
522 high values near islands more than for Chl; the corresponding pixels on the Chl grid (i.e. outside  
523 of the Chl shallow mask) were interpolated using a median filter.

524 **Island-driven impacts on chlorophyll and primary production.** Island impacts were assessed  
525 by contrasting data in the IME region to data in a reference region (REF), defined as the closest  
526 N pixels from the island mask that do not belong to any IME region, where N is the number of  
527 pixels within the IME region excluding the shallow mask (Extended Fig. 1). When assessing the  
528 island impact on variables other than chlorophyll (i.e. primary production or PHYSAT), the  
529 region with the largest number of data pixels was adapted. Indeed, different datasets may have  
530 different data gaps, thus changing the number of data points in each region. To ensure that the  
531 number of data points remained identical in both regions, the region with most pixels was  
532 randomly subsampled to match the region with fewer pixels. The REF region was used to define  
533 the nearby Chl increase for each island (Chl\_max relative to average Chl within REF). Detecting  
534 IMEs using a high sensitivity is justified on a climatological basis where spatial variability is  
535 heavily smoothed by a 17-year average; however, weak increases could result from noise.  
536 Statistics in Table 1 are thus presented both for all IMEs (more exhaustive) and after excluding  
537 IMEs with Chl increases near islands below 10% (more conservative).

538 **PHYSAT.** The PHYSAT method<sup>37</sup> is based on daily, 4-km resolution normalized water-leaving  
539 radiance (primary variable measured by a satellite ocean color radiometer after atmospheric  
540 correction, for several wavelengths). First, spectral radiance anomalies (Ra) are computed by  
541 removing a reference spectrum function of Chl for the same pixel, ensuring that the first order  
542 chlorophyll signal is removed. Then, these anomalies are clustered using an automatic  
543 unsupervised classification approach (self-organizing maps), classifying daily Ra into 100  
544 “neuron groups” corresponding to a specific Ra spectral frequency shape and amplitude<sup>56</sup>. The  
545 number of neuron groups is reduced using phenological metrics to identify signals linked to  
546 specific phytoplankton assemblages<sup>38</sup>, termed “phenoclasses” (61 for PHYSAT applied to

547 MODIS-Aqua). A previous version of PHYSAT was applied to the SeaWiFS satellite and  
548 matched with coincident *in situ* phytoplankton data, which enabled SeaWiFS phenoclasses to be  
549 labeled with six broad phytoplankton groups<sup>57</sup>. Phytoplankton labels are also available for  
550 MODIS phenoclasses, through SeaWiFS/MODIS matchups during their overlapping period.  
551 Around half of MODIS phenoclasses remain unlabeled, but could be matched to phytoplankton  
552 groups as more samples become available. The most common phenoclasses present in the  
553 tropical Pacific were labeled and found to be dominated by *Prochlorococcus*, *Synechococcus*,  
554 and nanoplankton. Daily MODIS phenoclasses (4 km resolution, July 2002 - April 2018) were  
555 averaged as a monthly climatology of phenoclass occurrence frequency at each pixel; pixels  
556 shallower than 30 m were removed. The corresponding product was used to calculate the  
557 phenoclass composition (percentage of occurrence for each phenoclass) within each IME and  
558 REF region detected previously. Ecological metrics were only computed in IME and REF  
559 regions including at least 100 PHYSAT data pixels, to ensure adequate PHYSAT coverage. This  
560 represents around half of the detected IMEs.

561 **PHYSAT ecological metrics.** Classical ecological metrics were computed from phenoclass  
562 proportions averaged in each IME and REF region, by regarding each phenoclass as a “species”  
563 in mathematical equations for each index. In practice, each phenoclass can contain varying  
564 numbers of species. However, phytoplankton richness is relatively stable in the tropics<sup>11</sup>, so that  
565 the number of phytoplankton species belonging to each phenoclass should be relatively constant.  
566 Island impacts on phenoclass composition were assessed using the Bray-Curtis dissimilarity  
567 index<sup>58</sup> between each pair of IME and REF regions. The Bray-Curtis index can vary between 0  
568 and 1, where 0 would indicate that IME and REF have the same phenoclass composition, and 1  
569 that they do not share any phenoclasses. Island impacts on phenoclass diversity were assessed

570 using various biodiversity metrics: richness, Pielou's evenness<sup>59</sup>, and the Shannon index<sup>60</sup>. These  
571 metrics were computed in each IME and REF regions separately, and contrasted (similar to  
572 chlorophyll and primary production). Just like true species richness strongly depends on  
573 sampling effort, phenoclass richness increases with the number of pixels over which it is  
574 computed (see Fig. S3). Phenoclass richness was corrected by rarefaction to 100 pixels to enable  
575 direct statistical comparisons of richness across regions<sup>61</sup>. Computing biodiversity indices from  
576 satellite products of phytoplankton taxonomy is not new. A previous study computed global  
577 Shannon diversity metrics from PHYSAT six broad phytoplankton groups, identifying regional  
578 hotspots matching known biodiversity hotspots<sup>62</sup>. While precise biodiversity estimates require an  
579 extensive knowledge of the community, the De Monte index worked by capturing spatial  
580 heterogeneity in dominant phytoplankton groups, which was shown to be highly correlated to  
581 phytoplankton biodiversity in a model<sup>63</sup>. Here, by applying a similar method but using all 61  
582 phenoclasses, we are exploiting the full power of the PHYSAT algorithm and capturing a more  
583 precise picture of changes in phytoplankton taxonomy and biodiversity. This is a very powerful  
584 approach because it bypasses the need to identify phytoplankton taxonomy from space. While  
585 PHYSAT is only a proxy for phytoplankton taxonomy, broad phenoclass diversity patterns match  
586 published phytoplankton biodiversity patterns such as increasing richness with phytoplankton  
587 biomass in unproductive waters<sup>43</sup> (Extended Fig. 3).

## 588 **Data availability statement**

589 The main outputs of this study, including the island database, IME and REF masks, and IME  
590 impacts on chlorophyll, primary production, and PHYSAT, are available as a dataset hosted on  
591 Zenodo<sup>64</sup>. The PHYSAT climatology calculated for this paper is available there as well;  
592 PHYSAT is now being processed by ACRI (<https://www.acri-st.fr/>) and PHYSAT data will soon  
593 be publicly available from their website. Other data that support the findings of this study are  
594 available in various public repositories: <https://coastwatch.pfeg.noaa.gov/erddap/info/index.html>  
595 (MODIS chlorophyll concentration), <http://science.oregonstate.edu/ocean.productivity/index.php>  
596 (MODIS primary production), <https://www.ngdc.noaa.gov/mgg/shorelines/gshhs.html> (GSHHG  
597 coastline), [https://www.gebco.net/data\\_and\\_products/gridded\\_bathymetry\\_data/](https://www.gebco.net/data_and_products/gridded_bathymetry_data/) (GEBCO  
598 bathymetry). The Nunn et al. (2016) island database is available as an additional file  
599 accompanying their paper (<https://doi.org/10.1186/s40562-016-0041-8>).

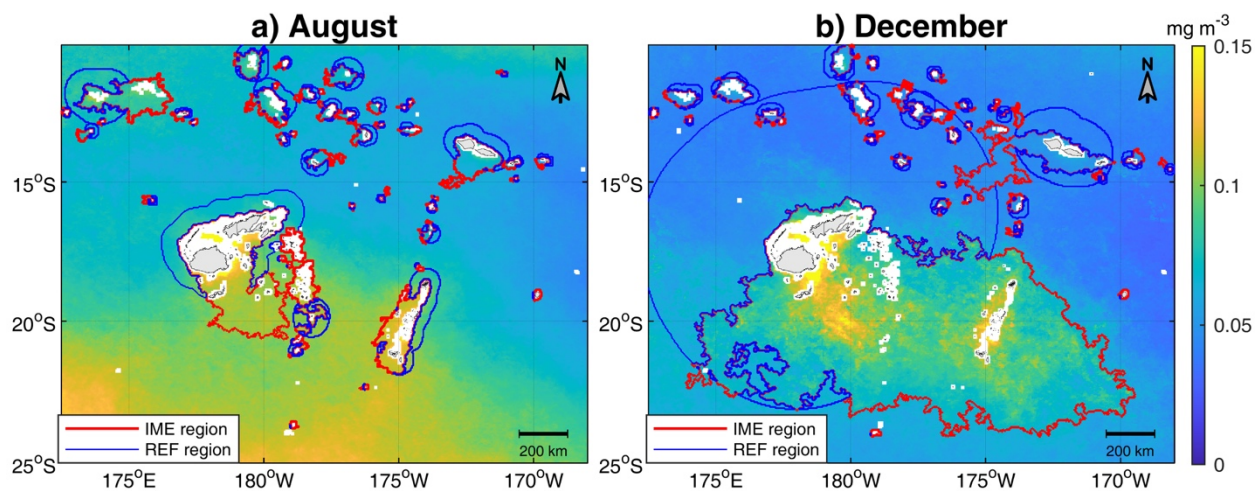
## 600 **Code availability statement**

601 The IME detection algorithm, along with datasets and example code to reproduce Fig. 1,  
602 Extended Fig. 1, and parts of Table 1, is available at  
603 [https://github.com/messiem/toolbox\\_IME\\_detection](https://github.com/messiem/toolbox_IME_detection) and the corresponding release published on  
604 Zenodo<sup>65</sup>.

605 **Additional references for the Methods section**

- 606 51. Nunn, P. D., L. Kumar, I. Eliot & R. F. McLean (2016), Classifying Pacific islands,  
607 Geoscience Letters, 3(1), <https://doi.org/10.1186/s40562-016-0041-8>
- 608 52. Hasegawa, D., M. R. Lewis & A. Gangopadhyay (2009), How islands cause phytoplankton  
609 to bloom in their wakes, Geophys. Res. Lett., 36, L20605,  
610 <https://doi.org/10.1029/2009GL039743>
- 611 53. Platt, T. & S. Sathyendranath (1988), Oceanic Primary Production: Estimation by Remote  
612 Sensing at Local and Regional Scales, Science, 241(4873), 1613-1620,  
613 <https://doi.org/10.1126/science.241.4873.1613>
- 614 54. Hasegawa, D., H. Yamazaki, T. Ishimaru, H. Nagashima & Y. Koike (2008), Apparent  
615 phytoplankton bloom due to island mass effect, J. Mar. Sys., 69(3-4), 238-246,  
616 <https://doi.org/10.1016/j.jmarsys.2006.04.019>
- 617 55. Silsbe, G. M., M. J. Behrenfeld, K. H. Halsey, A. J. Milligan & T. K. Westberry (2016), The  
618 CAFE model: A net production model for global ocean phytoplankton, Glob. Biogeochem.  
619 Cycles, 30(12), 1756-1777, <https://doi.org/10.1002/2016GB005521>
- 620 56. Ben Mustapha, Z., S. Alvain, C. Jamet, H. Loisel & D. Dessailly (2014), Automatic  
621 classification of water-leaving radiance anomalies from global SeaWiFS imagery:  
622 Application to the detection of phytoplankton groups in open ocean waters, Remote Sens.  
623 Environ., 146, 97-112, <https://doi.org/10.1016/j.rse.2013.08.046>
- 624 57. Alvain, S., C. Moulin, Y. Dandonneau & H. Loisel (2008), Seasonal distribution and  
625 succession of dominant phytoplankton groups in the global ocean: A satellite view, Glob.  
626 Biogeochem. Cycles, 22(3), <https://doi.org/10.1029/2007GB003154>

- 627 58. Bray, J. R. & J. T. Curtis (1957), An Ordination of the Upland Forest Communities of  
628 Southern Wisconsin, *Ecological Monographs*, 27(4), 325-349,  
629 <https://doi.org/10.2307/1942268>
- 630 59. Pielou, E. (1966), The measurement of diversity in different types of biological collections, *J.*  
631 *Theor. Biol.*, 13, 131-144, [https://doi.org/10.1016/0022-5193\(66\)90013-0](https://doi.org/10.1016/0022-5193(66)90013-0)
- 632 60. Shannon, C. & W. Weaver (1948), Biodiversity measurements, *The Mathematical Theory of*  
633 *Communication*. Urbana University Press, Illinois, 117-27
- 634 61. Colwell, R. K., C. X. Mao & J. Chang (2004), Interpolating, extrapolating, and comparing  
635 incidence-based species accumulation curves, *Ecology*, 85(10), 2717-2727,  
636 <https://doi.org/10.1890/03-0557>
- 637 62. De Monte, S., A. Soccodato, S. Alvain & F. d'Ovidio (2013), Can we detect oceanic  
638 biodiversity hotspots from space?, *The ISME Journal*, 7(10), 2054-2056,  
639 <https://doi.org/10.1038/ismej.2013.72>
- 640 63. Soccodato, A., F. d'Ovidio, M. Lévy, O. Jahn, M. J. Follows & S. D. Monte (2016),  
641 Estimating planktonic diversity through spatial dominance patterns in a model ocean, *Mar.*  
642 *Geonomics*, 29, 9-17, <https://doi.org/10.1016/j.margen.2016.04.015>
- 643 64. Messié, M., A. Petrenko, A. Doglioli, E. Martinez & S. Alvain (2022), Data from: Basin-  
644 scale biogeochemical and ecological impacts of islands in the tropical Pacific Ocean (v1.0.0),  
645 Zenodo, <https://doi.org/10.5281/zenodo.6416130>
- 646 65. Messié, M. (2022), Code for: Basin-scale biogeochemical and ecological impacts of islands  
647 in the tropical Pacific Ocean (v1.0.0), Zenodo, <https://doi.org/10.5281/zenodo.6494328>
- 648



649

650 **Extended Data Fig. 1: Example maps of IME and reference (REF) region detection. Two**

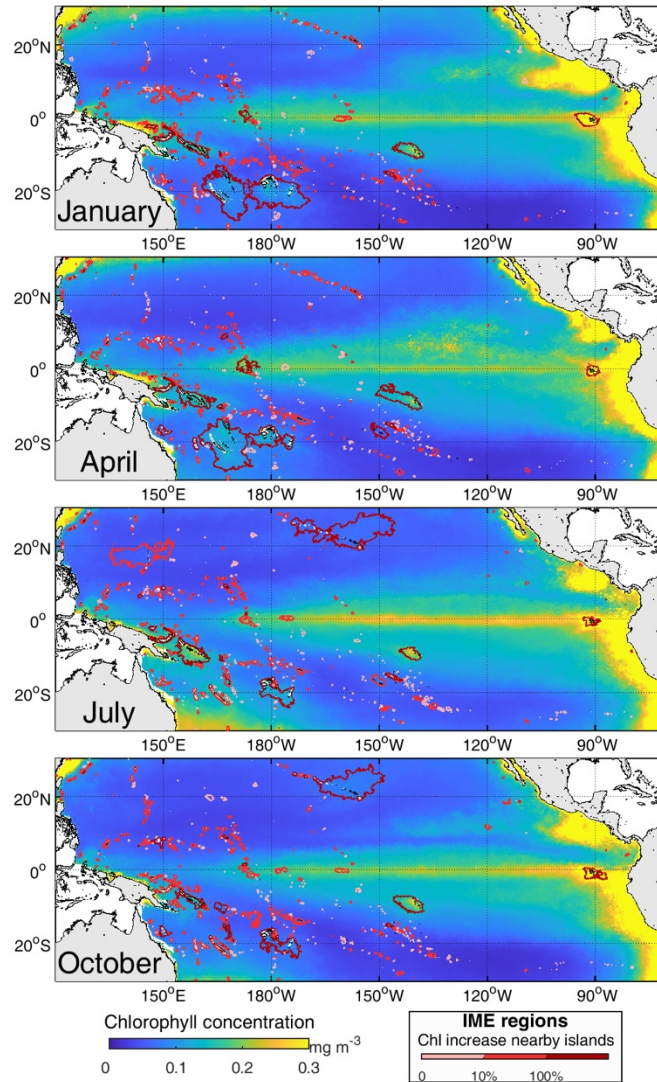
651 contrasting months are shown for the Fiji/Tonga region: a) August (small IMEs but higher

652 climatological enrichment across the region), and b) December (strong IMEs, with IMEs from

653 the Fiji and Tonga island groups merging). Reference regions (blue) exclude IME regions from

654 any island.

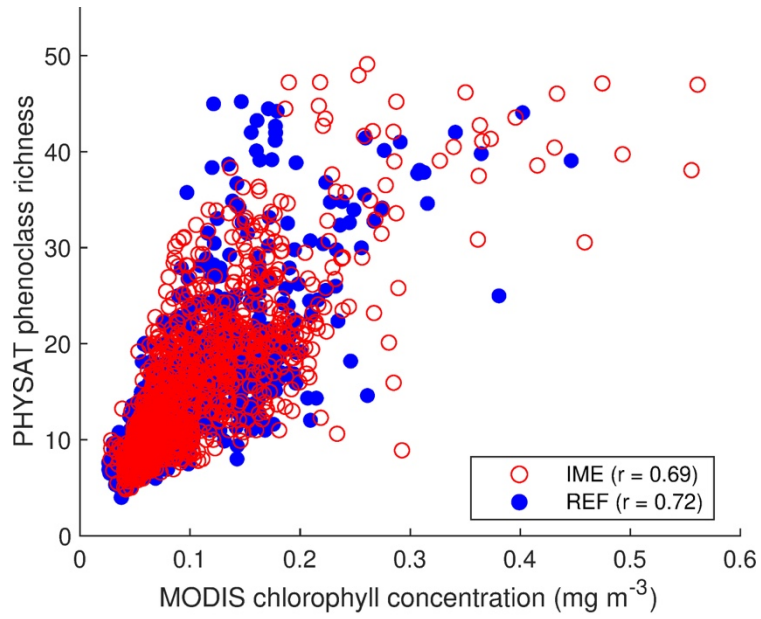
655



656

657 **Extended Data Fig. 2: IME maps for different climatological months.** For each month, IME  
 658 regions are contoured in different shades of red depending on Chl increase near islands relative  
 659 to a reference region (similar to Fig. 1).

660



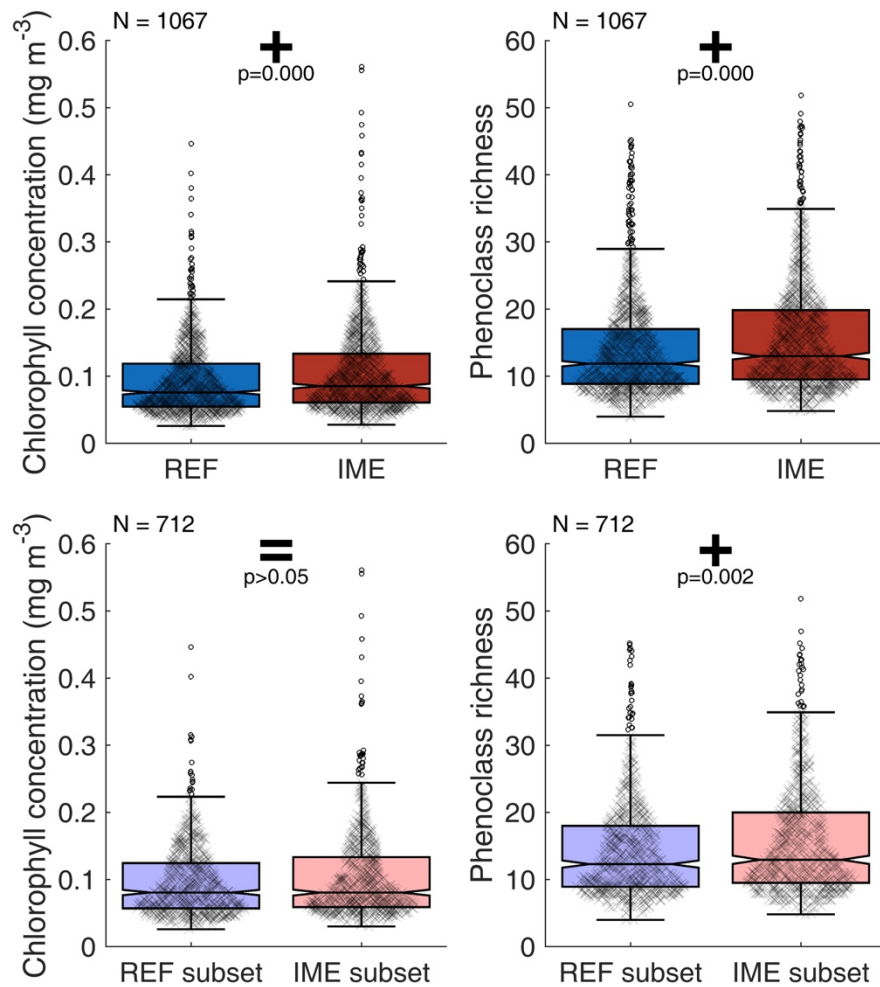
661

662 **Extended Data Fig. 3: PHYSAT phenoclass richness vs Chl across IME and REF regions.**

663 Phenoclass richness was normalized to 100 data points, and only regions with at least 100

664 PHYSAT data points were included.

665



666

667 **Extended Data Fig. 4: Example of random permutation used to remove the Chl signal on**  
 668 **the phenoclass richness increase observed in IME regions.** Top panel: identical to Fig. 3b left  
 669 panels (that is, including all IME and REF regions); both Chl (left) and phenoclass richness  
 670 (right) are significantly higher in IME than in REF regions (Mann-Whitney U-test). Bottom  
 671 panel: example of a random permutation where 2/3 of the IME and REF regions were retained  
 672 such that the Chl distributions do not significantly differ anymore. In this permutation,  
 673 phenoclass richness remains significantly higher within the IME subset (right) even though Chl  
 674 is (non-significantly) lower (left).

675

	All IMEs	IMEs with Chl increase nearby islands $\geq 10\%$
<b>IME spatial impact</b>		
IME area (in km <sup>2</sup> )	559 [172 – 2,051]	1,333 [430 – 3,965]
<b>IME impact on Chl</b>		
Nearby percentage Chl increase (in %)	11.4 [6.5 – 22.3]	19.9 [13.8 – 36.4]
Percentage Chl increase per IME (in %)	6.8 [4.4 – 10.8]	10.0 [7.3 – 14.2]
Total Chl increase per IME (in tons/m)	0.00 [0.00 – 0.01]	0.01 [0.00 – 0.04]
<b>IME impact on primary production (PP)</b>		
Percentage PP increase per IME (in %)	1.5 [0.3 – 3.5]	2.6 [0.9 – 5.3]
Total PP increase per IME (in TgC /yr)	0.00 [0.00 – 0.00]	0.00 [0.00 – 0.01]
<b>IME impact on PHYSAT phenoclass diversity</b>		
Percentage richness increase per IME (in %)	7.7 [-0.1 – 18.9]	8.9 [0.0 – 20.8]
Percentage evenness increase per IME (in %)	-0.3 [-6.4 – 6.0]	-0.3 [-6.6 – 6.2]
Percentage Shannon index increase per IME (in %)	2.9 [-1.7 – 8.7]	3.3 [-1.5 – 9.4]

676 **Extended Data Table 1: Additional metrics for IME impacts in the tropical Pacific (see**  
677 **Table 1).** Values are given as median [25th percentile – 75th percentile]. The extremely low  
678 values for total Chl and total primary production (intentionally kept in the same unit as in Table  
679 1) highlight how a few major IMEs (visible in Fig. 1) are responsible for most of the large-scale  
680 impact on Chl and primary production.